Light: A new handle to control the structure of cesium lead iodide

Charles Paillard [1,*] and Laurent Bellaiche[2]

[1]*Université Paris-Saclay, CentraleSupélec, CNRS, Laboratoire SPMS, 91190, Gif-sur-Yvette, France*
[2]*Department of Physics and Institute for Nanosciences, University of Arkansas, Fayetteville, Arkansas 72701, USA*

$CsPbI_3$ is of high interest for photovoltaic applications owing to its low band gap, provided it could be stabilized in its γ perovskite phase. Instead, it energetically prefers to adopt a so-called yellow, δ phase, with a much larger band gap and reduced photovoltaic properties. Here, using an original constrained density functional theory method, we mimic the effect of thermalized photoexcited carriers, and show that larger concentrations in photoexcited carriers (i.e., larger optical pump fluences) effectively reduce the energy difference between the δ nonperovskite ground state and the γ perovskite phase. Even further, the stability of the phases could be potentially reversed and therefore the γ phase stabilized under strong illumination. We also report large photostriction, i.e., large photoinduced strain for all phases in this material, making $CsPbI_3$ suitable for other applications such as photodriven relays and photoactuators.

I. INTRODUCTION

Halide perovskites represent a hope to achieve efficient and affordable solar power conversion. They have quickly grown to achieve more than 25% power conversion efficiency [1]. Their domain of application extends far beyond the mere solar cell, as their good photo- or electroluminescent properties [2,3] make them prime candidates for laser or light-emitting diode applications [4,5]. However, many of those halide perovskites suffer from severe stability issues with respect to humidity or temperature, in particular when they are made of a hybrid of organic–inorganic cations [6]. As a result, the fully inorganic lead halide perovskites, $CsPbX_3$ (X = I, Br, Cl), have been considered most promising owing to their greater stability [7]. Among those, $CsPbBr_3$ significantly starts absorbing at wavelengths below 550 nm (green), while $CsPbCl_3$ absorbs in the near-UV spectral domain. [2] As a result, those two compounds are not particularly promising to convert efficiently the solar spectrum into useful energy.

On the other hand, the perovskite phase of $CsPbI_3$ absorbs wavelengths as high as 700 nm [2]. Unfortunately, lead cesium iodide is only metastable in a perovskite phase; the more stable δ phase has much worse optical absorption properties [8]. The instability of the perovskite phase has recently been elucidated to stem from rattling of the Cs ion in its coordination cage, based on X-ray diffraction measurements on single crystals from 100 K to 295 K [9]. The perovskite phase can nonetheless be stabilized by substituting some I^- with Br^- at the expense of degraded absorption properties [2], or metastabilized through cooling from the high-temperature phase [10]. Yet, temperature and pressure are slow, cumbersome, and energy-inefficient control parameters. Methods allowing to easily and efficiently control the appearance of the perovskite phase in $CsPbI_3$ are thus highly desirable.

In the present work, we study the relative stability of the main four phases of $CsPbI_3$: the δ phase, which is the nonperovskite ground state; the γ phase, which is the low-energy orthorhombic perovskite phase; the β phase, an intermediate tetragonal perovskite structure; and the α phase, the cubic prototypical and high-temperature perovskite. All four phases are depicted in the Supplemental Material [24].

Density functional theory (DFT) calculations are employed in an original scheme which constrains excited electrons (resp. holes) in the conduction (resp. valence) bands during the self-consistent cycle to mimic thermalized photoexcited carriers. Our results indicate that above the band gap light may help tune the relative stability of the γ and δ phases. Even further, knowing that the γ phase is dynamically stable in dark conditions [11], our results may provide a pathway to trigger a transition to the perovskite phase without having to realize heavy and slow thermal cycles [10]. Furthermore, a large photoinduced strain is also calculated in all phases and in particular in the *stable* δ phase, where it is of high importance to use $CsPbI_3$ in photostrictive devices [12].

II. METHODS

In order to study the possibility of triggering a phase transition towards a perovskite phase in $CsPbI_3$, we used the constrained-DFT scheme developed in Ref. [13] as implemented by ABINIT [14–18], with a plane wave cutoff of 40 Ha. The Perdew-Burke-Ernzerhof (PBE) exchange correlation functional revised for solids (named PBESol) was employed. All calculations reported here include spin-orbit coupling (SOC). Plane augmented wave (PAW) pseudopotentials were regenerated for PBESol using the PBE pseudopotential parameters used in the Jollet-Torrent-Holzwarth (v1.1) table [19,20] and the ATOMPAW software [21]. The discretization of
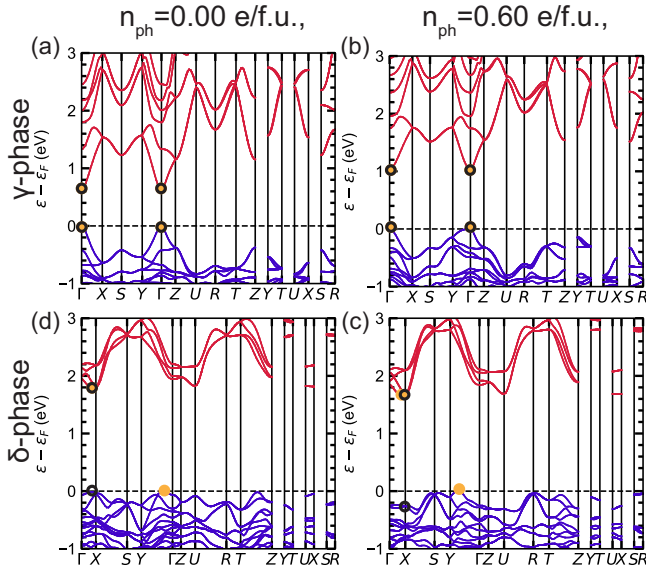
*charles.paillard@centralesupelec.fr

FIG. 1. Band structures obtained in the γ (a and b) and δ (c and d) phases for $n_{ph} = 0.00$ e/f.u. (electronic ground state, a and c) and $n_{ph} = 0.6$ e/f.u. (b and d), respectively; orange plain circles indicate the location of the electronic band gap, and black empty circles depict the direct band gap.

the Brillouin zone was performed using a Γ-centered mesh having 7×10^{-3} Bohr^{-1} sampling density along each reciprocal lattice vector direction. Self-consistent field cycles were considered converged when the difference in forces between two iterations was smaller than 10^{-8} Ha Bohr^{-1}; structural relaxation was performed until the maximum calculated force laid below 5×10^{-7} Ha Bohr^{-1}. Fermi-Dirac distributions with a smearing temperature of 0.004 Ha characterize the occupation of electronic states. The lattice constants obtained in the electronic ground state are in good agreement with lattice constants measured experimentally or calculated using the local density approximation (LDA) [22,23] (see Supplemental Material [24]). The reciprocal space paths used for the band structures for Fig. 1 are detailed in Ref. [25] In order to simulate photoexcitation, we constrained a finite number n_{ph} of electrons (resp. holes) to lie in the conduction (resp. valence) bands with a Fermi-Dirac distribution characterized by two separate quasi-Fermi levels for photoexcited electrons and holes.

III. PHOTOINDUCED PHASE TRANSITIONS

A. Structural and electronic properties in dark

We start by describing the electronic and energetic properties of CsPbI$_3$ in "dark" conditions ($n_{ph} = 0$). The band structures of the δ and γ phases are depicted in Figs. 1(a) and 1(d). The γ phase [Fig. 1(a)] has a direct band gap of 0.63 eV located at the Γ point. The electronic band gap of the δ phase is indirect and 1.79 eV large. The top of the valence band is located on the $Y\Gamma$ segment, while the bottom of the conduction band is close to X. The direct band gap, depicted with black empty circles, is located near X in reciprocal space, and is 1.80 eV large. In Table I, we summarize the values of band

TABLE I. Summary of electronic band gaps, in eV, of different phases in CsPbI$_3$.

	δ phase		γ phase
	$E_{g,\text{indirect}}$	$E_{g,\text{direct}}$	$E_{g,\text{direct}}$
This work, PBESol, SOC	1.79	1.80	0.63
This work, PBESol, no SOC	2.37	2.48	1.59
Ref. [28], PBE	–	–	1.78
Ref. [29], PBE	–	2.56	–
Ref. [30], PBE	–	2.6	1.75
Ref. [31], Exp	–	–	1.68
Ref. [9], Exp	–	2.58	1.63

gaps for the γ and δ phases, and compare with experimental and theoretical works. The predicted band gaps calculated with SOC underestimate both experimental and theoretical values obtained without SOC, as consistent with the literature [26,27,32].

The energy of the four phases without photoexcitation is depicted in Fig. 2 (see points at $n_{ph} = 0$). The lowest-energy structure is the δ phase, which lies below the γ phase by roughly 80 meV/f.u. This qualitatively differs from Ref. [22], but agrees well with experimental observations of the δ phase being the most stable state. The difference with Ref. [22] might be due to a different exchange-correlation functional used. We note, furthermore, that the relative energies of the phases δ, γ, β, and α agree well with the observed phase transitions upon cooling [8,10,23,33,34].

B. Energetics of phases under photoexcitation

Upon increasing the relative concentration of photoexcited carriers n_{ph}, the energy difference between the δ phase and γ phase (teal circles in Fig. 2) significantly decreases, and even changes sign at 0.3 e/f.u. This indicates that (i) for concentrations lower than 0.3 e/f.u, the transition temperature between the δ and γ phases will potentially decrease when
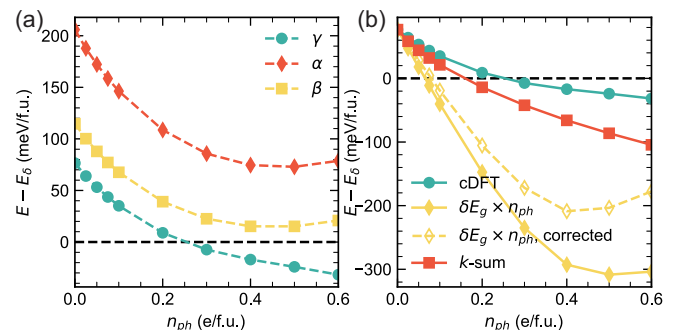

FIG. 2. (a) Energy of the α, β, and γ phases relative to the δ phase as a function of the concentration of photoexcited carriers; (b) Comparison between the constrained-DFT calculations (teal circles), the toy model given in Eq. (1) (yellow diamonds), the toy model corrected using the experimental band gaps (yellow dashed diamonds), and numerical integration (red squares) of the population of the "dark" band structures electronic states (see Appendix A for details.)

illuminating the sample with above-band-gap light and large fluence; and (ii) a potential phase transition from the yellow δ phase to the perovskite γ phase could occur under sufficiently intense illumination with above-band-gap energy photons. For a thin film, such concentration is reachable with high-intensity lasers. Prior experiments on MAPbI$_3$ [35] and a simple model (see Appendix A) indicate that laser pulses of 25 mJ cm^{-2} fluence and 3 eV photon energy may achieve these large concentration of photoexcited carriers. None of the other known phases of CsPbI$_3$ seem to become more stable in the range of concentrations in photoexcited carriers explored here.

We now attempt to elucidate the origin of this potential photoinduced phase transition. In other perovskites, mostly oxides and ferroelectrics, previous works showed that photoexcited carriers had a strong impact on phonon instabilities [13,36]. In particular, in cubic lead titanate and barium titanate, it had been found that phonon instabilities related to the development of electrical polarization were suppressed under illumination [13]. Here, the phonon spectrum of the cubic α phase (see Supplemental Material [24]) shows that photoexcited carriers hardly modify the unstable phonon branches. This is consistent with the fact that no other perovskite phase becomes more stable than the γ phase in Fig. 2. There does not seem to be any other perovskite phase that could develop under illumination besides the γ phase, which is itself dynamically stable [11].

C. Toy model

As a result, the case could be made that the proposed phase transition origin lies in the difference of electronic band gaps of the δ and γ phases. In a two-level system (e.g., limiting ourselves to the bottom of the valence band and top of the conduction band), a simple toy model can be designed to further prove this point. Akin to the extension of Landau's theory to the description of degenerate semiconductors [37] or to explain photostriction in ferroelectric oxides [38], one may simply say that the difference of energy between the two phases is

$$E_\gamma(n_{\text{ph}}) - E_\delta(n_{\text{ph}}) = \Delta E_0 + \delta E_g(n_{\text{ph}})n_{\text{ph}} \qquad (1)$$

In the above equation, ΔE_0 is the energy difference between the δ and γ phase in "dark" conditions (roughly 80 meV/f.u.); $\delta E_g(n_{\text{ph}}) = E_{g,\gamma}(n_{\text{ph}}) - E_{g,\delta}(n_{\text{ph}})$ denotes the difference of band gaps between the γ and δ phases, and n_{ph} represents the concentration of photoexcited carriers. We plot that quantity in Fig. 2(b) as filled yellow diamonds. It can be seen that qualitatively the result of the *ab initio* calculations and those obtained from Eq. (1) are similar. This supports the scenario of an electronically controlled energy difference between the two phases. Quantitative discrepancies between the model in Eq. (1) and DFT results stem from the fact that the photoexcited carriers are distributed across more than one level and one k point owing to the finite smearing temperature. One should, in fact, integrate over the (partially) occupied conduction (and valence) states in order to obtain a better match. The integration over the ground state band structure is depicted in red squares in Fig. 2(b) and detailed in Appendix B. The agreement is quantitatively better, and the remaining difference with constrained-DFT calculations

is likely to stem from some band reconfiguration under illumination.

Note that, because our calculations underestimate the band gap of CsPbI$_3$, the critical concentration of photoexcited carriers is likely underestimated. We used our toy model [see Eq. (1)] with experimental values of the band gaps of the γ and δ phases. The corrected curve, in dashed yellow diamonds in Fig. 2(b), slightly increases the critical n_{ph} of the transition. Interestingly, we also performed some calculations without SOC (see Supplemental Material [24]). In such case, the band gaps of both the δ and γ phases match the experimental ones well. The transition is then observed at a larger concentration of photoexcited carriers (~ 0.6 e/f.u.), as expected from the electronic nature of the photoinduced phase transition. The true critical concentration would be better determined using more accurate and costly exchange-correlation functionals.

Given the electronic nature of the proposed phase transition, one might wonder whether the formation of excitons could hinder the present phenomenon. Indeed, we have so far treated the photoexcited electrons and holes using a one-body Hamiltonian provided by the Kohn-Sham implementation of DFT. We note, however, that the exciton binding energy in CsPbI$_3$ reported in magnetooptical experiments is fairly small, of the order of 15 meV [39]; likewise, calculations report values in the range 1.5–44 meV [40,41]. In other words, and in particular at noncryogenic temperatures, excitons will mostly dissociate into photoexcited free carriers. Note also that we need demanding numerical criteria to obtain well-converged results, which is incompatible with the use of larger supercells. Consequently, the tendency of hybrid perovskites to disorder and to adopt medium-range correlations [42,43], and how these latter react to illumination, are not explored in this work. At last, we focused on phases which were previously experimentally reported. It is possible, although no evidence points in that direction, that other unknown phases could be accessed in CsPbI$_3$ under illumination. The use of genetic algorithms coupled to the constrained-DFT method used in this work could reveal such phases.

IV. PHOTOSTRICTION

We also looked at the photostrictive response of CsPbI$_3$. It is given in Table II, in which estimates use the value of the photoinduced strain at $n_{\text{ph}} = 0.025$ e/f.u. in Fig. 3. We chose such a value because it is small enough to be in a linear regime for most phases in CsPbI$_3$. Consequently, we plot, in Fig. 3, the photoinduced strain for all four phases of CsPbI$_3$ considered in this work. a, b, and c refer to the lattice constants of the principal axes sorted by increasing length. In the case of the α cubic phase for which $a = b = c$, we report only a, while for the β tetragonal phase, $a = b \neq c$, and we report only a and c. Interestingly, and as also summarized in Table II, the δ phase exhibits the largest photostrictive response. Compared to calculations of bulk oxides such as BiFeO$_3$ [44], PbTiO$_3$ [38], or the brownmillerite SrCoO$_{2.5}$ [45], CsPbI$_3$ exhibits superior photostrictive properties in all of its phases. Note that in Table II, the photostriction of rhombohedral BiFeO$_3$ reports that of the pseudocubic cell parameter, calculated using the self-consistent field (ΔSCF) method in Table 1 of Ref. [44], similar to rhombohedral BaTiO$_3$ [38]. Note also that in

TABLE II. Estimates of the linear photoinduced strain in lead cesium iodide calculated using the constrained-DFT method (no SOC/SOC values reported). Other reported compounds were calculated using the ΔSCF method.

Material	Phase	$\delta a/a$	$\delta b/b$ %/(e/f.u.)	$\delta c/c$
CsPbI$_3$	α	−0.02	–	–
	β	0.5	–	−0.8
	γ	0.2	1.4	1.5
	δ,	−9.9	15.3	−5.1
BiFeO$_3$ (perovskite [44])	$R3c$	−1.5	–	–
BaTiO$_3$ (perovskite [38])	$R3m$	−0.2	–	–
PbTiO$_3$ (perovskite [38])	$P4mm$	−1.0	–	−3.1
SrCoO$_{2.5}$ (brownmillerite [45])	$Ima2$	–	–	+0.4
SnS (2D ferroelectric [46])		−56.9	14.2-28.4	–

Table II we report photoinduced strains from ΔSCF calculations [38,44,46] corresponding to indirect transitions to match as closely as possible the results that would be obtained using the constrained-DFT method employed here.

We must also stress that at large concentrations in photoexcited carriers ($n_{ph} > 0.1$ e/f.u.), the photoinduced response can become highly nonlinear, especially in the β and α phases. While large photoinduced strain is observed across all phases in the large n_{ph} regime, Fig. 3 and Table II show that the δ phase possesses the largest photomechanical sensitivity under low-illumination conditions.

A recent study has attributed the large photostriction in *cubic* cesium lead halide perovskite to the strong antibonding nature of the bottom of the conduction band [47]. Our results indicate that the strong photoinduced strain permeates through all phases of CsPbI$_3$, at least in the large n_{ph} regime. The large photoinduced strain in CsPbI$_3$, and in general in hybrid perovskites [48], may find applications in improving the photovoltaic power conversion efficiency [49]. Interestingly,
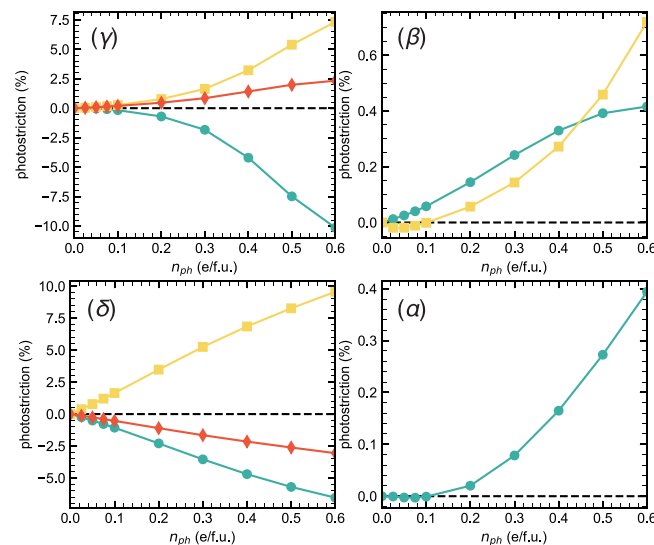
FIG. 3. Photoinduced strain in lead cesium iodide, along the principal crystallographic axes of each phase (γ, β, δ, and α). Dashed open symbols in the δ and γ phases show calculations with SOC.
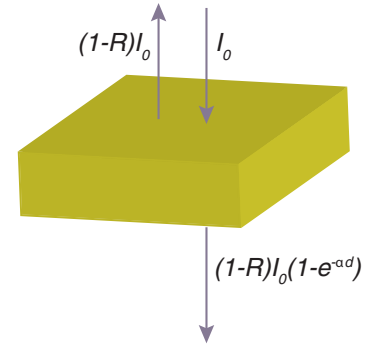
FIG. 4. Sketch of what happens to a ray of light of intensity I_0 impinging on a material.

to achieve photostriction comparable to the 0.125% expansion reported in MAPbI$_3$ films [48], one could use 413 nm wavelength laser pulses of 8.5 mJ cm^{-2}.

V. CONCLUSION

The constrained-DFT approach employed in the present study unveils that thermalized photoexcited carriers can reduce, and even invert, the relative energy difference between the δ phase and the γ perovskite phase of CsPbI$_3$. This allows to envision new ways to transform into or better stabilize the γ phase, which is highly important for photovoltaic applications. In particular, the present work proposes that visible light could trigger a photoinduced phase transition towards the γ perovskite phase, which is of high interest for photovoltaic applications. Once the phototransition is achieved and the light removed, it is likely that the γ phase will remain kinetically stable since it has already been proven to be metastable under dark conditions using thermal quenching [10,50]. It is unclear at present whether CsPbI$_3$ could sustain the proposed intensity to reach the phase transition. Working near the yellow-to-black phase transition temperature should lower the critical value of light intensity necessary to reach the transition. Conversely, one could expect that using visible illumination (for instance with lasers) will lower the transition temperature, leading to more efficient and ecological manufacturing of CsPbI$_3$-based devices. In addition, our calculations reveal that CsPbI$_3$ is an efficient photostrictive material, especially in the δ phase, which was previously thought to be a detrimental phase with respect to photovoltaic applications. This work may thus pave the way for other and easier applications of CsPbI$_3$ in photoactuators.
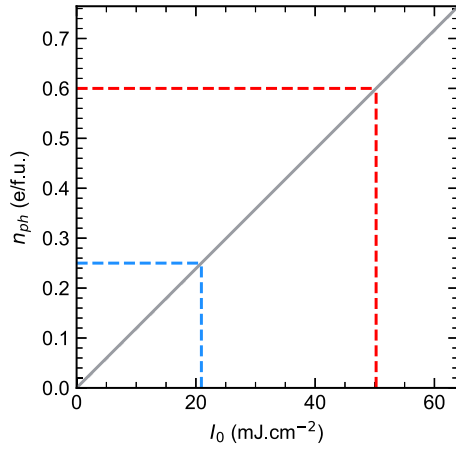
FIG. 5. Estimated photoinduced carrier concentration induced by a 3 eV laser pulse. Dotted blue and red lines correspond to the concentration necessary to achieve the $\delta \longrightarrow \gamma$ transition with and without SOC, according to Fig. 2 of the main manuscript.

APPENDIX A: PHOTOINDUCED CARRIER ESTIMATE

We estimate the photoexcited carrier concentration. Considering the power balance sketched in Fig. 4, the total absorbed energy from a laser of fluence I_0 impinging on a sample of cross section S, thickness d, having absorption and reflection coefficient α and R, is

$$E_{\mathrm{tot}} = (1 - R)I_0(1 - e^{-\alpha d})S. \tag{A1}$$

As a result, the total number of photons absorbed is

$$N_{\mathrm{photons}} = \frac{E_{\mathrm{tot}}}{\hbar\omega} = \frac{(1 - R)I_0(1 - e^{-\alpha d})S}{\hbar\omega}, \tag{A2}$$

with $\hbar\omega$ the average photon energy within the incident beam. Assuming that each absorbed photon yields an electron-hole pair, we would thus have a photoexcited carrier density, expressed in e/f.u., of

$$n_{\mathrm{ph}} = \frac{N_{\mathrm{photons}}}{Sd} \times \frac{V_\delta}{4}, \tag{A3}$$

where V_δ is the volume of the δ phase unit cell. The factor $1/4$ comes from the fact that there are four formula units in the δ phase unit cell.

Assuming, for the sake of simplicity, that photons in the laser beam carry an energy $\hbar\omega = 3$ eV (413 nm), we take for the δ phase a value of $\alpha \approx 2 \times 10^5$ cm^{-1} [8]. We take a reflection coefficient $R = 0.15$, similar to what can be found in CsPbBr$_3$ thin films, a parent compound [51]. This allows us to obtain a crude estimate of the value of n_{ph} depending on the

pump fluence, which we plot in Fig. 5. Note that in Fig. 5, we assumed a sample uniformly illuminated of thickness 323 nm, area size $S = 0.0625$ cm^2, which is submitted to a laser pulse carrying an energy up to 4 mJ. The geometrical parameters involved were taken from photostriction experiments carried out on thin films of MAPbI$_3$ [35]. One observes that reasonable pulse energy can lead to the desired concentration of photoexcited carriers in thin films.

Note that in the previous simple derivations, we assumed that every electron-hole pair relaxes into thermalized carriers in their respective bands (valence bands for holes; conduction bands for electrons). We also assume that the recombination time of excited carriers is large enough compared to the pulse duration. Typical relaxation times in CsPbI$_3$ are of the order of a few nanoseconds [52,53] (depending on the sample quality). Picosecond laser pulses could therefore be suitable for this model. A more complex model would solve a balance equation or the real time Bethe-Salpether equation to obtain a more accurate relation between the pump fluence and the average number of photoexcited carriers.

APPENDIX B: NUMERICAL INTEGRATION AND TOY MODEL

One can understand the physical mechanisms at play using a simple toy model. It is detailed in Eq. (1). This allows us to consider completely flat conduction and valence bands, i.e., a two-level system. To further refine our model, we performed a numerical integration of the ground state band structures. In other words, we consider a model (denoted as "k-sum" in the main manuscript) of the form

$$E_\gamma(n_{\mathrm{ph}}) - E_\delta(n_{\mathrm{ph}}) = \Delta E_0 + \left\{ \left[E_c^\gamma(n_{\mathrm{ph}}) - E_v^\gamma(n_{\mathrm{ph}}) \right] - \left[E_c^\delta(n_{\mathrm{ph}}) - E_v^\delta(n_{\mathrm{ph}}) \right] \right\}. \tag{B1}$$

$E_{\gamma/\delta}^c(n_{\mathrm{ph}})$ represents the electronic energy change due to the electrons in the conduction band, and can be expressed as

$$E_c^{\gamma/\delta}(n_{\mathrm{ph}}) = \sum_k \sum_c w_k f\left(\varepsilon_{k,c}^{\gamma/\delta}, \mu_e, T \right) \varepsilon_{k,c}^{\gamma/\delta}, \tag{B2}$$

where c represents the conduction band index, k the k point in the irreducible discretized Brillouin zone, w_k its weight, μ_e the electronic quasi-Fermi level, T the smearing temperature, and $\varepsilon_{k,c}^{\gamma/\delta}$ the eigenvalue of k point k with band index c, taken in the γ/δ phase calculated with $n_{\mathrm{ph}} = 0$ e/f.u. $f(\varepsilon_{k,c}^{\gamma/\delta}, \mu_e, T)$ represents the Fermi-Dirac population of this state with energy $\varepsilon_{k,c}^{\gamma/\delta}$. Similarly, $E_{\gamma/\delta}^v(n_{\mathrm{ph}})$ is the energy change caused by the presence of holes in the valence bands.

[1] J. Jeong, M. Kim, J. Seo, H. Lu, P. Ahlawat, A. Mishra, Y. Yang, M. A. Hope, F. T. Eickemeyer, M. Kim, Y. J. Yoon, I. W. Choi, B. P. Darwich, S. J. Choi, Y. Jo, J. H. Lee, B. Walker, S. M. Zakeeruddin, L. Emsley, U. Rothlisberger *et al.*, Pseudo-halide anion engineering for α-FAPbI3 perovskite solar cells, Nature (London) **592**, 381 (2021).

[2] L. Protesescu, S. Yakunin, M. I. Bodnarchuk, F. Krieg, R. Caputo, C. H. Hendon, R. X. Yang, A. Walsh, and M. V. Kovalenko, Nanocrystals of cesium lead halide perovskites

(CsPbX3, X = Cl, Br, and I): Novel optoelectronic materials showing bright emission with wide color gamut, Nano Lett. **15**, 3692 (2015).

[3] F. Liu, Y. Zhang, C. Ding, S. Kobayashi, T. Izuishi, N. Nakazawa, T. Toyoda, T. Ohta, S. Hayase, T. Minemoto, K. Yoshino, S. Dai, and Q. Shen, Highly luminescent phase-stable CsPbI3 perovskite quantum dots achieving near 100% absolute photoluminescence quantum yield, ACS Nano **11**, 10373 (2017).

[4] S.-T. Ha, R. Su, J. Xing, Q. Zhang, and Q. Xiong, Metal halide perovskite nanomaterials: Synthesis and applications, Chem. Sci. **8**, 2522 (2017).

[5] L. Chouhan, S. Ghimire, C. Subrahmanyam, T. Miyasaka, and V. Biju, Synthesis, optoelectronic properties and applications of halide perovskites, Chem. Soc. Rev. **49**, 2869 (2020).

[6] A. Senocrate, G. Y. Kim, M. Grätzel, and J. Maier, Thermo-chemical stability of hybrid halide perovskites, ACS Energy Lett. **4**, 2859 (2019).

[7] W. Xiang, S. F. Liu, and W. Tress, A review on the stability of inorganic metal halide perovskites: Challenges and opportunities for stable solar cells, Energy Environ. Sci. **14**, 2090 (2021).

[8] S. Valastro, G. Mannino, E. Smecca, S. Sanzaro, I. Deretzis, A. L. Magna, A. K. Jena, T. Miyasaka, and A. Alberti, Optical behaviour of γ-black CsPbI$_3$ phases formed by quenching from 80°C and 325°C, J. Phys. Mater. **4**, 034011 (2021).

[9] D. B. Straus, S. Guo, A. M. Abeykoon, and R. J. Cava, Understanding the instability of the halide perovskite CsPbI$_3$ through temperature-dependent structural analysis, Adv. Mater. **32**, 2001069 (2020).

[10] J. A. Steele, H. Jin, I. Dovgaliuk, R. F. Berger, T. Braeckevelt, H. Yuan, C. Martin, E. Solano, K. Lejaeghere, S. M. J. Rogge, C. Notebaert, W. Vandezande, K. P. F. Janssen, B. Goderis, E. Debroye, Y.-K. Wang, Y. Dong, D. Ma, M. Saidaminov, H. Tan, Thermal unequilibrium of strained black CsPbI$_3$ thin films, Science **365**, 679 (2019).

[11] A. Jain, S. P. Ong, G. Hautier, W. Chen, W. D. Richards, S. Dacek, S. Cholia, D. Gunter, D. Skinner, G. Ceder, and K. A. Persson, The Materials Project: A materials genome approach to accelerating materials innovation, APL Mater. **1**, 011002 (2013).

[12] B. Kundys, Photostrictive materials, Appl. Phys. Rev. **2**, 011301 (2015).

[13] C. Paillard, E. Torun, L. Wirtz, J. Íñiguez, and L. Bellaiche, Photoinduced Phase Transitions in Ferroelectrics, Phys. Rev. Lett. **123**, 087601 (2019).

[14] X. Gonze, B. Amadon, G. Antonius, F. Arnardi, L. Baguet, J.-M. Beuken, J. Bieder, F. Bottin, J. Bouchet, E. Bousquet, N. Brouwer, F. Bruneval, G. Brunin, T. Cavignac, J.-B. Charraud, W. Chen, M. Côté, S. Cottenier, J. Denier, G. Geneste *et al.*, The ABINIT project: Impact, environment and recent developments, Comput. Phys. Commun. **248**, 107042 (2020).

[15] A. H. Romero, D. C. Allan, B. Amadon, G. Antonius, T. Applencourt, L. Baguet, J. Bieder, F. Bottin, J. Bouchet, E. Bousquet, F. Bruneval, G. Brunin, D. Caliste, M. Côté, J. Denier, C. Dreyer, P. Ghosez, M. Giantomassi, Y. Gillet, O. Gingras *et al.*, ABINIT: Overview and focus on selected capabilities, J. Chem. Phys. **152**, 124102 (2020).

[16] X. Gonze, F. Jollet, F. Abreu Araujo, D. Adams, B. Amadon, T. Applencourt, C. Audouze, J.-M. Beuken, J. Bieder, A. Bokhanchuk, E. Bousquet, F. Bruneval, D. Caliste, M. Côté, F. Dahm, F. Da Pieve, M. Delaveau, M. Di Gennaro, B. Dorado, C. Espejo *et al.*, Recent developments in the ABINIT software package, Comput. Phys. Commun. **205**, 106 (2016).

[17] M. Torrent, F. Jollet, F. Bottin, G. Zérah, and X. Gonze, Implementation of the projector augmented-wave method in the ABINIT code: Application to the study of iron under pressure, Comput. Mater. Sci. **42**, 337 (2008).

[18] F. Bottin, S. Leroux, A. Knyazev, and G. Zérah, Large-scale *ab initio* calculations based on three levels of parallelization, Comput. Mater. Sci. **42**, 329 (2008).

[19] F. Jollet, M. Torrent, and N. Holzwarth, Generation of projector augmented-wave atomic data: A 71 element validated table in the XML format, Comput. Phys. Commun. **185**, 1246 (2014).

[20] JTH -v1.1 table (2021), https://www.abinit.org/downloads/PAW2.

[21] N. Holzwarth, A. Tackett, and G. Matthews, A Projector Augmented Wave (PAW) code for electronic structure calculations, Part I: atompaw for generating atom-centered functions, Comput. Phys. Commun. **135**, 329 (2001).

[22] A. Marronnier, G. Roma, S. Boyer-Richard, L. Pedesseau, J.-M. Jancu, Y. Bonnassieux, C. Katan, C. C. Stoumpos, M. G. Kanatzidis, and J. Even, Anharmonicity and disorder in the black phases of cesium lead iodide used for stable inorganic perovskite solar cells, ACS Nano **12**, 3477 (2018).

[23] D. Liu, Z. Shao, C. Li, S. Pang, Y. Yan, and G. Cui, Structural properties and stability of inorganic CsPbI$_3$ perovskites, Small Struct. **2**, 2000089 (2021).

[24] See Supplemental Material at http://link.aps.org/supplemental/10.1103/PhysRevB.107.054107, where crystallographic structures, comparison of SOC and no SOC calculations, and phonon instabilities in the cubic perovskite phase are presented (2021).

[25] W. Setyawan and S. Curtarolo, High-throughput electronic band structure calculations: Challenges and tools, Comput. Mater. Sci. **49**, 299 (2010).

[26] J. Even, L. Pedesseau, J.-M. Jancu, and C. Katan, Importance of spin–orbit coupling in hybrid organic inorganic perovskites for photovoltaic applications, J. Phys. Chem. Lett. **4**, 2999 (2013).

[27] J. Brgoch, A. J. Lehner, M. Chabinyc, and R. Seshadri, *Ab initio* calculations of band gaps and absolute band positions of polymorphs of RbPbI$_3$ and CsPbI$_3$: Implications for main-group halide perovskite photovoltaics, J. Phys. Chem. C **118**, 27721 (2014).

[28] M. A. Fadla, B. Bentria, T. Dahame, and A. Benghia, First-principles investigation on the stability and material properties of all-inorganic cesium lead iodide perovskites CsPbI$_3$ polymorphs, Phys. B: Condens. Matter **585**, 412118 (2020).

[29] L.-K. Gao and Y.-L. Tang, Theoretical study on the carrier mobility and optical properties of CsPbI$_3$ by DFT, ACS Omega **6**, 11545 (2021).

[30] I. Deretzis, C. Bongiorno, G. Mannino, E. Smecca, S. Sanzaro, S. Valastro, G. Fisicaro, A. La Magna, and A. Alberti, Exploring the structural competition between the black and the yellow phase of CsPbI$_3$, Nanomaterials **11**, 1282 (2021).

[31] S. Xu, A. Libanori, G. Luo, and J. Chen, Engineering bandgap of CsPbI$_3$ over 1.7 eV with enhanced stability and transport properties, iScience **24**, 102235 (2021).

[32] J.-C. Tung, Y.-H. Hsieh, and P.-L. Liu, Strain induced topological insulator phase in CsPbBr$_x$I$_{3-x}$ ($x = 0$, 1, 2, and 3) perovskite: A theoretical study, Appl. Sci. **11**, 5353 (2021).

[33] R. J. Sutton, M. R. Filip, A. A. Haghighirad, N. Sakai, B. Wenger, F. Giustino, and H. J. Snaith, Cubic or orthorhombic? Revealing the crystal structure of metastable black-phase CsPbI$_3$ by theory and experiment, ACS Energy Lett. **3**, 1787 (2018).

[34] H. Yao, H. Zhao, Z. Li, Z. Ci, and Z. Jin, Research and progress of black metastable phase CsPbI$_3$ solar cells, Mater. Chem. Front. **5**, 1221 (2021).

[35] X. Du, J. Li, G. Niu, J.-H. Yuan, K. -H. Xue, M. Xia, W. Pan, X. Yang, B. Zhu, and J. Tang, Lead halide perovskite for efficient optoacoustic conversion and application toward high-resolution ultrasound imaging, Nat. Comm. **12**, 3348 (2021).

[36] B. Peng, Y. Hu, S. Murakami, T. Zhang, and B. Monserrat, Topological phonons in oxide perovskites controlled by light, Sci. Adv. **6**, eabd1618 (2020).

[37] R. E. Pasynkov, On some problems of the phenomenological theory of ferroelectric-semiconductors, Ferroelectrics **6**, 19 (1973).

[38] C. Paillard, S. Prosandeev, and L. Bellaiche, *Ab initio* approach to photostriction in classical ferroelectric materials, Phys. Rev. B **96**, 045205 (2017).

[39] Z. Yang, A. Surrente, K. Galkowski, A. Miyata, O. Portugall, R. J. Sutton, A. A. Haghighirad, H. J. Snaith, D. K. Maude, P. Plochocka, and R. J. Nicholas, Impact of the halide cage on the electronic properties of fully inorganic cesium lead halide perovskites, ACS Energy Lett. **2**, 1621 (2017).

[40] P. Basera, A. Singh, D. Gill, and S. Bhattacharya, Capturing excitonic effects in lead iodide perovskites from many-body perturbation theory, J. Mater. Chem. C **9**, 17113 (2021).

[41] M. R. Filip, J. B. Haber, and J. B. Neaton, Phonon Screening of Excitons in Semiconductors: Halide Perovskites and Beyond, Phys. Rev. Lett. **127**, 067401 (2021).

[42] X. G. Zhao, G. M. Dalpian, Z. Wang, and A. Zunger, Polymorphous nature of cubic halide perovskites, Phys. Rev. B **101**, 155137 (2020).

[43] X. Wang, K. Patel, S. Prosandeev, Y. Zhang, C. Zhong, B. Xu, and L. Bellaiche, Finite-temperature dynamics in cesium lead iodide halide perovskite, Adv. Funct. Mater. **31**, 2106264 (2021).

[44] C. Paillard, B. Xu, B. Dkhil, G. Geneste, and L. Bellaiche, Photostriction in Ferroelectrics from Density Functional Theory, Phys. Rev. Lett. **116**, 247401 (2016).

[45] B. Zhang, X. He, J. Zhao, C. Yu, H. Wen, S. Meng, E. Bousquet, Y. Li, C. Ge, K. Jin, Y. Tao, and H. Guo, Giant photoinduced lattice distortion in oxygen vacancy ordered SrCoO$_{2.5}$ thin films, Phys. Rev. B **100**, 144201 (2019).

[46] R. Haleoot, C. Paillard, T. P. Kaloni, M. Mehboudi, B. Xu, L. Bellaiche, and S. Barraza-Lopez, Photostrictive Two-Dimensional Materials in the Monochalcogenide Family, Phys. Rev. Lett. **118**, 227401 (2017).

[47] B. Peng, D. Bennett, I. Bravić, and B. Monserrat, Tunable photostriction of halide perovskites through energy dependent photoexcitation, Phys. Rev. Mater. **6**, L082401 (2022).

[48] Y. Zhou, L. You, S. Wang, Z. Ku, H. Fan, D. Schmidt, A. Rusydi, L. Chang, L. Wang, P. Ren, L. Chen, G. Yuan, L. Chen, and J. Wang, Giant photostriction in organic–inorganic lead halide perovskites, Nat. Commun. **7**, 11193 (2016).

[49] H. Tsai, R. Asadpour, J.-C. Blancon, C. C. Stoumpos, O. Durand, J. W. Strzalka, B. Chen, R. Verduzco, P. M. Ajayan, S. Tretiak, J. Even, M. A. Alam, M. G. Kanatzidis, W. Nie, and A. D. Mohite, Light-induced lattice expansion leads to high-efficiency perovskite solar cells, Science **360**, 67 (2018).

[50] G. E. Eperon, G. M. Paternò, R. J. Sutton, A. Zampetti, A. A. Haghighirad, F. Cacialli, and H. J. Snaith, Inorganic caesium lead iodide perovskite solar cells, J. Mater. Chem. A **3**, 19688 (2015).

[51] W. Yan, L. Mao, P. Zhao, A. Mertens, S. Dottermusch, H. Hu, Z. Jin, and B. S. Richards, Determination of complex optical constants and photovoltaic device design of all-inorganic CsPbBr$_3$ perovskite thin films, Opt. Express **28**, 15706 (2020).

[52] S. Dastidar, S. Li, S. Y. Smolin, J. B. Baxter, and A. T. Fafarman, Slow electron–hole recombination in lead iodide perovskites does not require a molecular dipole, ACS Energy Lett. **2**, 2239 (2017).

[53] C. de Weerd, L. Gomez, A. Capretti, D. M. Lebrun, E. Matsubara, J. Lin, M. Ashida, F. C. Spoor, L. D. Siebbeles, A. J. Houtepen, K. Suenaga, Y. Fujiwara, and T. Gregorkiewicz, Efficient carrier multiplication in CsPbI$_3$ perovskite nanocrystals, Nat. Commun. **9**, 4199 (2018).